JACS
JOURNAL OF THE AMERICAN CHEMICAL SOCIETY
Article
pubs.acs.org/JACS

# Fine-Tuning of β-Substitution to Modulate the Lowest Triplet Excited States: A Bioinspired Approach to Design Phosphorescent Metalloporphyrinoids

Xian-Sheng Ke,[†] Hongmei Zhao,[‡] Xiaoran Zou,[‡] Yingying Ning,[†] Xin Cheng,[†] Hongmei Su,*[,‡,§] and Jun-Long Zhang*[,†,∥]

[†]Beijing National Laboratory for Molecular Sciences, State Key Laboratory of Rare Earth Materials Chemistry and Applications, College of Chemistry and Molecular Engineering, Peking University, Beijing 100871, P.R. China

[‡]Beijing National Laboratory for Molecular Sciences, Institute of Chemistry, Chinese Academy of Sciences, Beijing 100190, P.R. China

[§]College of Chemistry, Beijing Normal University, Beijing 100875, P.R.China

[∥]State Key Laboratory of Coordination Chemistry, Nanjing University, Nanjing, 210093, P.R. China

Supporting Information

**ABSTRACT:** Learning nature's approach to modulate photophysical properties of NIR porphyrinoids by fine-tuning β-substituents including the number and position, in a manner similar to naturally occurring chlorophylls, has the potential to circumvent the disadvantages of traditional "extended π-conjugation" strategy such as stability, molecular size, solubility, and undesirable π−π stacking. Here we show that such subtle structural changes in Pt(II) or Pd(II) *cis/trans*-porphodilactones (termed by ***cis/trans*-Pt/Pd**) influence photophysical properties of the lowest triplet excited states including phosphorescence, Stokes shifts, and even photosensitization ability in triplet−triplet annihilation reactions with rubrene. Prominently, the overall upconversion capability ($\eta$, $\eta = \varepsilon \cdot \Phi_{UC}$) of Pd or Pt trans-complex is $10^4$ times higher than that of cis-analogue. Nanosecond time-resolved infrared (TR-IR) spectroscopy experiments showed larger frequency shift of $\nu$(C═O) bands (ca. 10 $cm^{-1}$) of cis-complexes than those of trans-complexes in the triplet excited states. These spectral features, combining with TD-DFT calculations, suggest the strong electronic coupling between the lactone moieties and the main porphyrin chromophores and thus the importance of precisely positioning β-substituents by mimicking chlorophylls, as an alternative to "extended π-conjugation", in designing NIR active porphyrinoids.

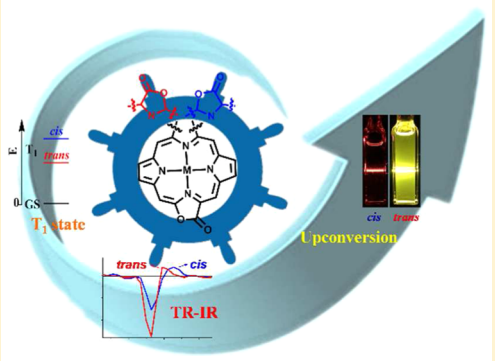


## INTRODUCTION

Design of porphyrinoids active in the near-infrared (NIR) region is an ever expanding field with potential impacts in areas from fundamental understanding of natural tetrapyrrole cofactors to diverse applications in materials, biological studies, and related fields.[1] Owing to electronic structures conferred by π-conjugation system, β-peripheral substituents of porphyrinoids are particularly attractive design targets and such modification is an emerging approach because of the tantalizing prospect of introducing new functionality and control of photophysical properties. The well-established "extended π-conjugation" strategies in synthetic porphyrin chemistry,[2] exemplified by tetrabenzoporphyrins and linearly π-expanded derivatives such as naphtho- and anthro-fused porphyrins, has been extensively demonstrated the efficiency to accumulatively extend NIR absorption and emission. However, the increasingly elevated HOMO levels along with π-conjugation extension and molecular sizes render these porphyrinoids unstable, poor solubility and π−π stacking between molecules.[3]

Naturally occurring tetrapyrrole pigments, such as Chl *a*, *b*, *d*, and *f*, have set a golden standard, which is capable of modulating NIR absorption (ca. 650−700 nm) by fine-tuning β-substitution with the broad structural similarity.[4] Such subtle structural changes inducing distinctive spectra related to ground states have been explicitly described in de novo synthetic chlorophyll analogues, in combination with density functional theory (DFT) calculations based Gouterman's four-orbital model.[5] Another notable bonus to nature's approach is minimizing the structural changes, avoiding the problems such as solubility, structural distortion, and undesirable π−π stacking. Despite the widespread recognition of the importance of β-substitution on the photophysics of chlorophylls,[4] few systematic studies on the effects of such β-substitution on the triplet excited states. Learning how to modulate the low-lying triplet states of porphyrinoids like chlorophylls, which prevents

**Received:** June 18, 2015
**Published:** August 6, 2015





DOI: 10.1021/jacs.5b06332
J. Am. Chem. Soc. 2015, 137, 10745−10752

transferring energy to oxygen instead of carotenoids and protect chlorophylls in NIR region, is equally important.[6] This would open new means to design NIR active porphyrinoids as optoelectronic materials, solar fuel and photosensitizers with large Stokes shift to reduce self-absorption and thus enhance energy transfer efficiency.

We previously reported porphodilactones with two β-oxazolone moieties replacing the pyrroles at opposite positions,[7] and demonstrated that relative orientation of such moieties affects electronic structures, NIR absorption and magnetic circular dichroism (MCD) spectra. In this work, we synthesized Pd(II) and Pt(II) complexes of *cis*- and *trans*-porphodilactones (termed by ***cis*/*trans*-Pd** and ***cis*/*trans*-Pt**), which display the gradually red-shifted absorption, NIR phosphorescence, and accumulative Stokes shifts, compared to metal complexes of tetrapentafluorophenylporphyrin ($F_{20}$TPP)[8] and porpholactone ($F_{20}$TPPL).[9] Importantly, ***trans*-Pt/Pd** showed red-shifted phosphorescence (ca. 30−57 nm) with longer life times (30−50%) than cis analogues, clearly suggesting the orientation of β-dioxazolone moieties not only modulate the ground states but the triplet excited states. More importantly, electrochemical studies combining with DFT calculation demonstrated that β-oxazolone replacement significantly influences LUMO rather than HOMO level, different from those in previously reported "π-expanded" porphyrinoids. Noticeably, nanosecond time-resolved infrared (TR-IR) spectroscopy experiments for ***cis*/*trans*-Pd/Pt** showed more frequency change of ν(C═O) bands (ca. 10 $cm^{-1}$) of cis complexes between ground and triplet excited states than trans complexes, indicating further the fine-tuning effect of cis/trans positioning on electronic structures. Finally, in triplet−triplet annihilation (TTA) reactions with rubrene, ***trans*-Pd** showed much higher delayed fluorescence quantum yield (1.0%) than ***cis*-Pd** (0.08%), strongly demonstrating that subtle structural changes induce significant sensitization enhancement in the NIR region. Therefore, these results herein presented reveal the importance of precisely positioning β-substituents in design NIR porphyrinoid emitters, which would be complementary to traditional "extended π-conjugation" strategies, with the advantages such as minimizing structural changes, good solubility, stability resistant to oxidation, and tunable emission in NIR region.

## RESULTS AND DISCUSSION

**Synthesis and Characterization.** *cis*- and *trans*-$H_2$ ($H_2$ = tetrapentafluorophenyl porphodilactone) free bases were prepared according to previously reported procedures.[7] Pt and Pd complexes were prepared by refluxing $M(acac)_2$ (M = Pt or Pd, 5 equiv, acac = acetylacetonate) with porphodilactone ligands in PhCN, yielding ***cis*/*trans*-Pt** and ***cis*/*trans*-Pd** in 10, 18, 43, and 45%, respectively (Scheme 1). The $^1$H NMR spectra of ***trans*-Pt/Pd** in $CDCl_3$ showed one β-H signal located in ca. δ = 8.67 ppm, whereas ***cis*-Pt/Pd** displayed more complicated β-H signals with two peaks at 8.52 and 8.62 ppm (***cis*-Pt**), and 8.46 and 8.59 ppm (***cis*-Pd**), respectively (Figure S9−12). $^{19}$F-NMR spectra of ***cis*/*trans*-Pt/Pd** showed that 20 F atoms located at 59.0−60.8, 71.5−72.6, and 82.2−83.3 ppm, using trifluoroacetic acid (TFA) as an external standard (Figure S13−16). $^{13}$C NMR spectra of ***cis*/*trans*-Pt/Pd** showed that carbon signals assigned for the C═O group are located at 161.9, 162.3, 162.1, and 162.3 ppm (Figure S17−20), respectively. Similar chemical shift of $^{13}$C NMR signals of C═O groups might indicate their similarity at the ground state

**Scheme 1. Synthetic Procedure for Pt(II) and Pd(II) Porphodilactones**

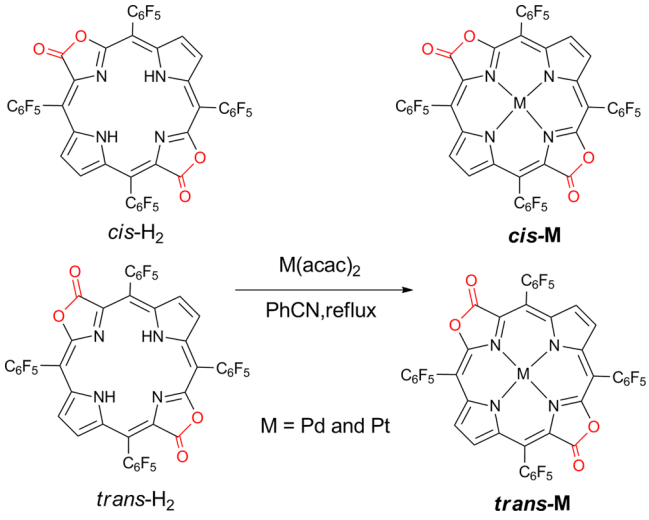


in cis/trans complexes. FT-IR spectra of ***cis*/*trans*-Pt/Pd** showed the characteristic C═O band vibrations based on the orientation of the β-dilactone moieties, in which trans complexes displays lower energy vibrations (1776 $cm^{-1}$ for ***trans*-Pt** and 1771 $cm^{-1}$ for ***trans*-Pd**) than cis complexes (1779 $cm^{-1}$ for ***cis*-Pt** and 1775 $cm^{-1}$ for ***cis*-Pd**; Figure S21−24). These spectral features are similar to those observed in *trans*- and *cis*-$H_2$ and their Zn complexes.[7] HR-ESI mass spectra of ***cis*/*trans*-Pt** and ***cis*/*trans*-Pd** showed the main peaks corresponding to $[M + H]^+$ or $[M]^+$ of 1203.9604, 1202.9560, 1113.8927, and 1113.8948, respectively, which is according to molecular weights based on the empirical formula (Figure S25−28).

Crystals suitable for X-ray diffraction for ***trans*/*cis*-Pt** were obtained. Crystallographic studies revealed that both complexes crystallized in monoclinic space group, with $C_2$ axis passing through the Pt atom, perpendicular to the porphyrinoid plane of ***trans*-Pt** and that lies in the plane of cis isomer. ***trans*-Pt** (CCDC: 1060750) clearly indicates the trans location of β-oxazolone moieties, whereas the oxygen atoms of carbonyl in ***cis*-Pt** (CCDC: 1060749) were found disordered toward two directions with equal proportions. As shown in Figure 1, for ***cis*/*trans*-Pt**, the Pt atom was located perfectly in the slightly distorted plane defined by the $N_4$ cavity. The mean Pt−N (oxazolone moieties) bond distance (1.992 Å) in ***cis*/*trans*-Pt** is slightly shorter than that in $PtF_{20}$TPP (2.018 Å)[8] and $PtF_{20}$TPPL (2.003 Å, CCDC:252892). In addition, relative orientation of the lactone moieties has slight effect on the C═O bond distances (1.153 and 1.196 Å, for ***cis*-** and ***trans*-Pt** respectively), which are slightly shorter than that in $PtF_{20}$TPPL (1.215 Å).

**Photophysical Properties.** The electronic absorption spectra of ***cis*/*trans*-Pt** and ***cis*/*trans*-Pd** in dichloromethane (DCM) exhibited intense Soret bands at 402−411 nm (Figure 2), with pronounced shoulders of intensity to the blue and low-energy Q bands at ca. 607−638 nm. Compared to Pd or Pt complexes of $F_{20}$TPP and $F_{20}$TPPL (Table S1), the lowest energetic Q(0,0) bands of ***cis*/*trans*-Pt** and ***cis*/*trans*-Pd** red-shift to 607, 623, 617, and 638 nm, respectively. Notable intense $Q_y$ bands were observed in ***trans*-Pt/Pd** and the extinction coefficient ratio of lowest energetic Q(0,0) band and Soret band ($\varepsilon_{Q(0,0)}/\varepsilon_{Soret}$) are 0.68 and 0.69, which are larger


DOI: 10.1021/jacs.5b06332
J. Am. Chem. Soc. 2015, 137, 10745−10752

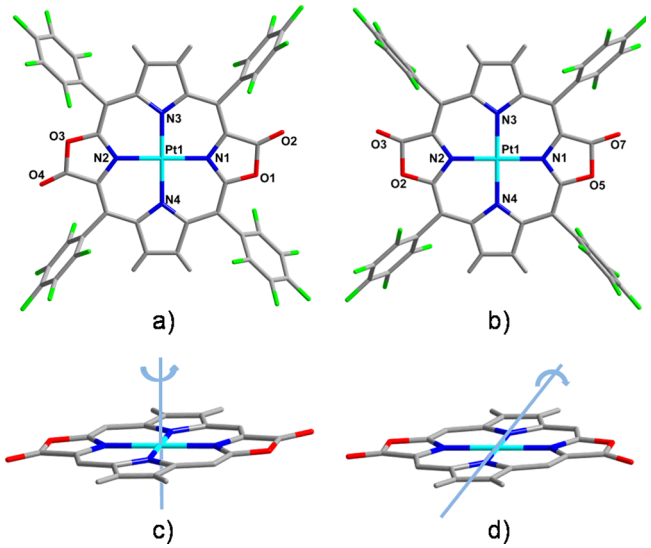


**Figure 1.** Stick models of the single crystal X-ray structures of (a) ***trans*-Pt** and (b) ***cis*-Pt**. The $C_2$ symmetry axis for (c) ***trans*-Pt** is perpendicular to the core porphyrin plane and (d) ***cis*-Pt** lies in the plane. The disorder of the oxygen atoms of carbonyl in ***cis*-Pt** was omitted.

than those in cis isomers (0.46 for ***cis*-Pt** and 0.34 for ***cis*-Pd**). The distinctive Q bands between trans and cis isomers suggest the orientation of $\beta$-oxazolone moieties are important to tune the energies of the frontier $\pi$-MOs, which are consistent to those observed in Zn porphodilactone complexes.[7]

Upon excitation in the Soret or Q-band region, ***cis*/*trans*-Pt**/**Pd** displayed an intense luminescence in the NIR region (836–916 nm) with a red-shifted shoulder (ca. 99–142 nm) (Figure 2). The measured lifetimes (10.9, 21.0, 83.0, and 109.9 $\mu$s for ***cis*/*trans*-Pt** and ***cis*/*trans*-Pd**, respectively) in the microsecond range suggest that the emission is probably of triplet parentage, giving rise to air-sensitive phosphorescence. As shown in Table 1, the phosphorescence quantum yields were determined as 0.04, 0.06, 0.01, and 0.01 for ***cis*/*trans*-Pt** and ***cis*/*trans*-Pd**, respectively, referred to ZnTPP ($\Phi$ = 0.033 in toluene[10]). Importantly, the modular and accumulative increases of Stokes shifts of either Pt or Pd complexes were observed (Table 1 and Figure S1), following the trend of porphyrin, porpholactone to *cis*/*trans*-porphodilactones. Such Stokes shifts are comparable to those obtained in Pt complexes of $\beta$-aryl fused porphyrins series of $\beta$-benzo- (161 nm), naphthalo- (202 nm) to anthro- (260 nm),[11] clearly suggesting the number and orientation of $\beta$-oxazolone moieties effectively influence the phosphorescence and thus triplet excited states of metalloporphyrinoids with the broad structural similarity.

The redox properties of ***cis*/*trans*-Pt/Pd**, together with their porphyrin and porpholactone analogues, in DCM were examined by cyclic voltammetry using tetra-*n*-butylammonium hexafluorophosphate ($n$-$Bu_4NPF_6$) assupporting electrolyte (Figure S1–2). Electrochemical data listed in Table S2 revealed that $\beta$-lactonization in the sequence $PtF_{20}TPPL$, ***cis*-** and ***trans*-Pt** results in gradual anodic shifting of the first reduction

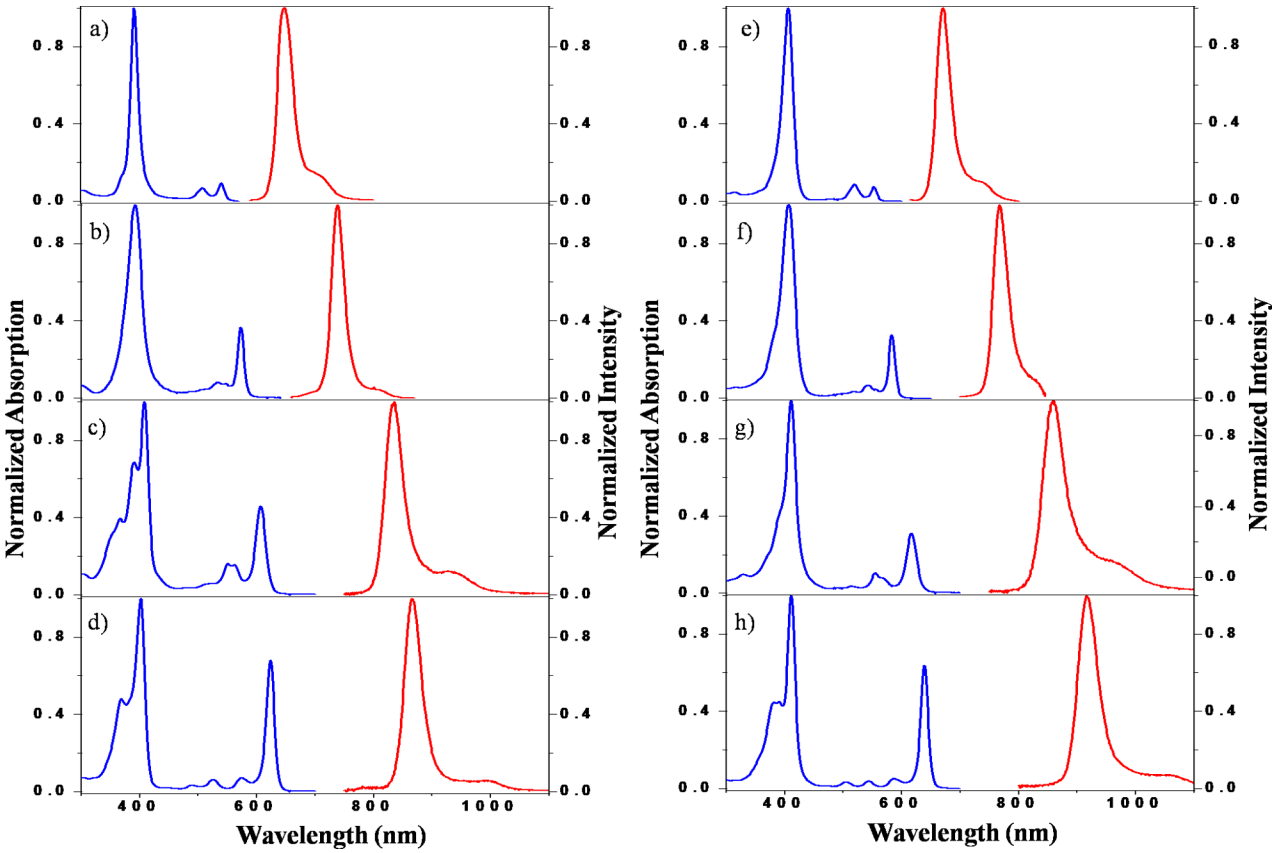


**Figure 2.** UV–vis (blue) and phosphorescence (red) spectra of (a) $PtF_{20}TPP$, (b) $PtF_{20}TPPL$, (c) ***cis*-Pt**, (d) ***trans*-Pt**, (e) $PdF_{20}TPP$, (f) $PdF_{20}TPPL$, (g) ***cis*-Pd**, and (h) ***trans*-Pd** in DCM at room temperature. The sample for the phosphorescence spectra measurements were through 5 freeze–pump–thaw cycles.



DOI: 10.1021/jacs.5b06332
J. Am. Chem. Soc. 2015, 137, 10745–10752

**Table 1. Photophysical Data of Pt(II) and Pd(II) Porphodilactone**

| | UV−vis $\lambda_{max}$ [nm] (log $\varepsilon$ [$M^{-1}$ $cm^{-1}$]) | | | | |
|---|---|---|---|---|---|
| | Soret bands | Q bands | phosphorescence[a] $\lambda_{max}$ [nm] ($\tau$ [$\mu$s]) | $\Phi_p$[b] | Stokes shift [nm] |
| ***cis*-Pt** | 366 (4.71),391 (4.94), 408 (5.10) | 550 (4.32), 562 (4.30), 607 (4.76) | 836 (10.9), 935 | 0.04 | 229 |
| ***trans*-Pt** | 369 (4.87), 402 (5.18) | 488 (3.83), 525 (4.06), 574 (4.05), 623 (5.04) | 866 (21.0), 1000 | 0.06 | 243 |
| ***cis*-Pd** | 411(5.22) | 514(3.81), 555(4.27), 568 (4.15), 617(4.75) | 859 (83.0), 969 | 0.01 | 242 |
| ***trans*-Pd** | 382(4.87), 391(4.87), 411(5.22) | 505(3.79), 543(3.85), 585 (3.98), 638(5.06) | 916(109.9), 1058 | 0.01 | 278 |

[a]Determined in degassed DCM solutions at room temperature. [b]Determined in degassed DCM solutions at room temperature with ZnTPP ($\Phi$ = 0.033 in toluene) as standard.

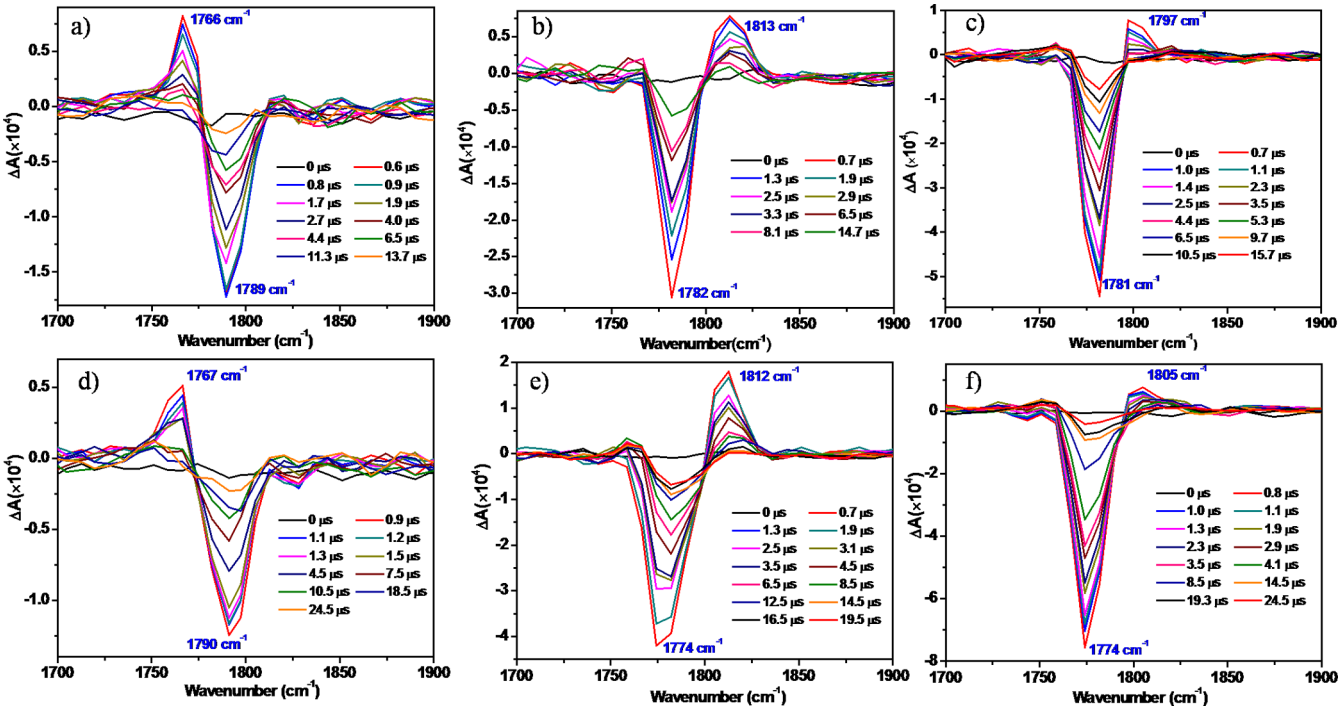


**Figure 3.** Nanosecond transient IR spectra of (a) $PtF_{20}TPPL$, (b) ***cis*-Pt**, (c) ***trans*-Pt**, (d) $PdF_{20}TPPL$, (e) ***cis*-Pd**, and (f) ***trans*-Pd** in $CH_3CN$ at selected time delays following 355 nm laser irradiation.

potentials of ca. 0.20, 0.37, and 0.46 V compared with $PtF_{20}TPP$, whereas negligible changes in the first oxidation potentials were observed. A similar trend was observed in the Pd series. As a consequence, the electrochemically determined HOMO−LUMO gaps for ***trans*-Pt/Pd** are smaller than those of their porphyrin or porpholactone or cis-isomer counterparts, consistent to the trend of DFT calculated HOMO−LUMO gaps. These results demonstrate that the replacement of pyrrole to $\beta$-oxazolone moiety is more effective to tune LUMO energy than HOMO and more resistant to oxidative condition, in contrast to those observed in "$\pi$-extension" NIR porphyrins, in which more increase of HOMO energy than LUMO.[3a−d]

**Time Resolved Infrared Spectroscopy and Computational Studies.** To gain further insights into the triplet excited state properties, we performed time-resolved infrared (TRIR) spectroscopy experiments for the characteristic C═O bond stretching vibrations of metalloporpholactones or metalloporphodilactones, which allows us to distinguish the nature of electronic structures related to the triplet states.[12] In the TRIR spectra of $PtF_{20}TPPL$ and ***cis*/*trans*-Pt** (Figure 3a−c) upon the irradiation of nanosecond 355 nm laser, the ground state bleaching bands of $PtF_{20}TPPL$ (1789 $cm^{-1}$), ***cis*-Pt** (1783 $cm^{-1}$), and ***trans*-Pt** (1781 $cm^{-1}$) were observed, in accompany with the appearance of positive bands for $PtF_{20}TPPL$ (1766 $cm^{-1}$), ***cis*-Pt** (1813 $cm^{-1}$), and ***trans*-Pt** (1797 $cm^{-1}$), which are air sensitive and microsecond scaled lifetimes. These positive bands are assigned to C═O stretching vibrations in the triplet states and match well with the theoretically predicted vibrational frequencies (Table S3). Similar TRIR results were obtained for $PdF_{20}TPPL$ and ***cis*/*trans*-Pd** (Figure 3d−f).

Comparison of the IR bands in the triplet state relative to ground state showed a remarkable difference between $MF_{20}TPPL$ and ***cis*/*trans*-M** (M = Pd and Pt). For example, the $\nu$(C═O) IR band of $PtF_{20}TPPL$ displayed a shift of 23 $cm^{-1}$ to the lower frequency in the triplet state compared to that in its ground state, whereas those for ***cis*-Pt** and ***trans*-Pt** showed 30 and 16 $cm^{-1}$ shifts to the higher frequency, respectively. Similar changes of $\nu$(C═O) IR bands (shift of 23 $cm^{-1}$ to the lower frequency for $PdF_{20}TPPL$ and shifts of 38 and 31 $cm^{-1}$ to the higher frequency for ***cis*/*trans*-Pd**, respectively) were observed for Pd complexes. It shows here that the C═O vibrational frequencies are sensitive to the electronic transition from the ground to the triplet excited states, suggesting the strong electronic coupling between the lactone moieties and the main porphyrin chromophores. Thus, the carbonyl group C═O introduced by $\beta$-lactonization can


DOI: 10.1021/jacs.5b06332
J. Am. Chem. Soc. 2015, 137, 10745−10752

serve as a vibrational signature to reflect the electronic structure change upon excitation. Moreover, the C═O vibrational frequency change from the $S_0$ state to the $T_1$ state is sensitive to the extent of $\beta$-lactonization and cis/trans positioning, demonstrating further fine-tuning ability of $\beta$-dioxazolone moieties on the excited state electronic structures. Generally, the hypsochromic shift in $\nu$(C═O) can be resulted from the inductive effect of the more highly electronegative substituent, such as nitrogen, oxygen, or halogen atom, while an extension of the conjugated system can cause bathochromic shift.[13] The inductive and conjugation effects can be further understood by the combined theoretical calculations as follows.

Hybrid density functional theory (B3LYP[14]) calculations were performed using cc-pvdz basis sets for C, N, H, F, and O atom and the LANL2DZ basis set[15] for Pt and Pd atom, taking into account the relativistic effects implicitly. Based on the optimized structures, the atomic polar tensors (APT) charge difference for $T_1$ and $S_0$ is first characterized, which can properly characterize the inductive effect.[16] Figure 4 shows the

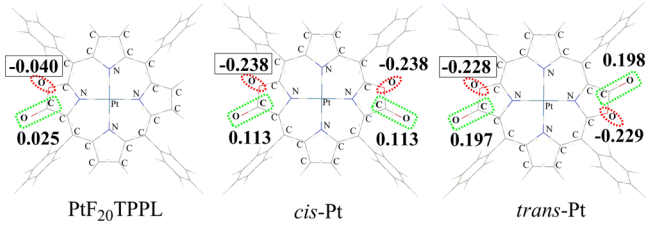


**Figure 4.** APT charge difference between triplet and singlet state calculated with the B3LYP functional.

APT charge difference on the carbonyl group and the adjacent oxygen between $T_1$ and $S_0$ for $PtF_{20}TPPL$, ***cis***- and ***trans*-Pt**. (For Pd porpholactones, similar results are provided in Figure S3). From $S_0$ to $T_1$, more negative charges are shown on the electron withdrawing oxygen, in accompany with the depletion of electron density on the carbonyl group. For ***cis***- and ***trans*-Pt**, obvious APT charge difference is shown on the substituent oxygen (−0.238 and −0.228), indicating strong inductive effect that may lead to the hypsochromic shift of $\nu$(C═O) for the triplet ***cis*-Pt** and ***trans*-Pt**. For $PtF_{20}TPPL$, the inductive effect is quite weak as shown by the small APT charge difference on the substituent oxygen (−0.04).

Additionally, molecular frontier orbital calculations were performed to characterize the conjugation effect, which also governs the C═O vibrational frequency. The promotion of an electron from HOMO to LUMO results in an electronic transition for singlet state, while the corresponding orbitals in the triplet manifold are the singly occupied molecular orbitals SOMO-1 and SOMO-2. The molecular orbital feature of SOMO-2 resembles LUMO (Figures S5 and S6), while SOMO-1 differs HOMO profoundly. Comparison of SOMO-1 ($T_1$) with HOMO ($S_0$) of $PtF_{20}TPPL$, ***cis*-Pt** and ***trans*-Pt** is shown in Figure 5. (Similar results for Pd porpholactones are provided in Figure S4.) For $PtF_{20}TPPL$, the conjugation along O−C−C in HOMO is extended to O−C−C-N in SOMO-1. This makes the carbonyl group to be of larger single bond character in the triplet state and thus the $\nu$(C═O) is shifted to lower frequency. Considering the weak inductive effect in $PtF_{20}TPPL$, the conjugation effect should become predominant and result in lowering of the triplet IR frequency in total, and a red-shift of 23 $cm^{-1}$ was indeed observed in the experiment. For ***cis*-Pt**, the O−C−C conjugation in HOMO and SOMO-1

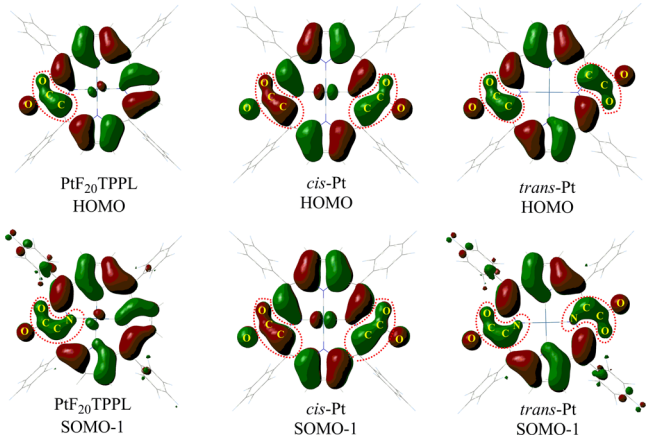


**Figure 5.** HOMO of singlet state and SOMO-1 of triplet state calculated with the B3LYP functional. Isovalue: 0.02.

are almost the same. Therefore, the triplet $\nu$(C═O) IR band is mainly blue-shifted due to the predominant inductive effect. For ***trans*-Pt**, the extension of conjugation from O−C−C in HOMO to O−C−C−-N in SOMO-1 is again displayed. This conjugation effect should then decrease the blue-shifts of the triplet $\nu$(C═O) IR band caused by the inductive effect and result in less total blue-shifts compared with ***cis*-Pt**, which is consistent with the TRIR spectral results that the triplet $\nu$(C═O) IR bands display blue-shifts of 30 $cm^{-1}$ for ***cis*-Pt** and 16 $cm^{-1}$ for ***trans*-Pt** (Figure 3).

Interestingly, the above analysis suggests that $\beta$-lactonization and cis/trans positioning play subtle roles in modulating the frontier molecular orbitals, through which the triplet electronic structures and energies are effectively tuned, as manifested by vibrational frequency shifts in TRIR spectra and phosphorescence wavelength shifts, respectively. As shown in Figure 5, the introduced O−C−C conjugation by $\beta$-lactonization favors decreasing the $T_1$-$S_0$ energy gap, and this energy gap is further reduced from cis to trans positioning because of the further conjugation extension from O−C−C in HOMO to O−C−C-N in SOMO-1 for ***trans*-Pt**. The trend of conjugation extension in frontier molecular orbitals coincides with the phosphorescence red-shifts of 90, 188, and 218 nm for $PtF_{20}TPPL$, ***cis*-Pt** and ***trans*-Pt** compared with $PtF_{20}TPP$, respectively. Furthermore, the calculated phosphorescence emission wavelength were consitent to experimental results (Table S4)

**Photosensitizing Property of Metalloporphodilactones in the NIR Region.** To demonstrate the potential application of metalloporphodilactones in thte NIR region, in this work, we chose rubrene as a triplet acceptor with a low-lying triplet state ($E_T$ = 1.14 eV) and performed triplet−triplet annihilation (TTA) reaction with ***cis*/*trans*-Pd** for the longer lifetime than Pt complexes.[17] Dynamic Stern−Volmer (S−V) analysis of triplet energy transfer rate constants of rubrene (acceptor) with ***cis*/*trans*-Pd** showed similar S−V constants of 1.80 and 1.81 × $10^5$ $M^{-1}$ for ***cis*/*trans*-Pd** (Figures S7−8), indicating rubrene has comparable quenching efficiency to the triplet states of ***cis*/*trans*-Pd**. As shown in Figure 6a, the preliminary results showed ***trans*-Pd** is most effective among ***cis*/*trans*-Pt/Pd** and emitted the strongest upconverted fluorescence from rubrene ($\lambda_{em}$ = 561 nm) upon excitation at 635 ± 5 nm.

Plotting emission intensity vs laser power density (635 ± 5 nm) reveals the nonlinear nature of the TTA process using


DOI: 10.1021/jacs.5b06332
J. Am. Chem. Soc. 2015, 137, 10745−10752

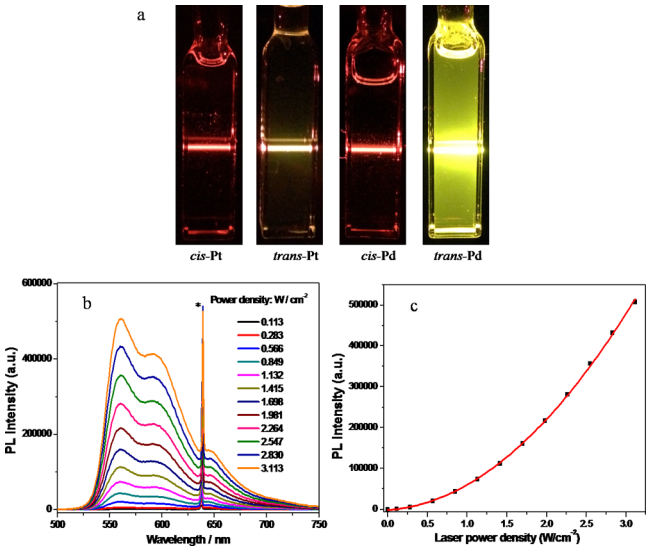


**Figure 6.** (a) Images of the upconverted fluorescence of rubrene with ***cis*-Pt**, ***trans*-Pt**, ***cis*-Pd**, and ***trans*-Pd** as sensitizers inside the 1 cm quartz cell (3.0 $\mu$M sensitizers and 180 $\mu$M acceptor, $\lambda_{ex}$ = 635 ± 5 nm, 55 mW, central wavelength located at 639 nm, no optical filters were used); (b) upconverted emission intensity profile of rubrene following selective excitation (635 ± 5 nm laser) of ***trans*-Pd** measured as a function of incident power density in degassed toluene; (c) emission intensity at 561 nm from panel b, plotted as a function of the incident light power. The asterisks in panel b indicate the scattered light of the excitation laser. The red line in panel c represents the best quadratic fit to the data.

***trans*-Pd** as a photosensitizer, which shows upconverted fluorescence intensity is proportional to the square of the incident light power (Figure 6b,c). The quantum yields of upconverted fluorescence ($\Phi_{UC}$) were determined relative to a methylene blue quantum counter ($\Phi_f$ = 0.030 in methanol[18]) with excitation at 635 ± 5 nm. $\Phi_{UC}$s are 0.037%, 0.18%, 0.076%, and 1.02% for ***cis*/*trans*-Pt/Pd**, respectively (Table 2).

**Table 2. Upconversion Quantum Yield ($\Phi_{UC}$) and Overall Upconversion Capability ($\eta$) of *cis*-Pt, *trans*-Pt, *cis*-Pd and *trans*-Pd with Rubrene**

| sensitizers | $\Phi_{UC}$[a] (%) | $\eta$[b] ($M^{-1}cm^{-1}$) |
|---|---|---|
| ***cis*-Pt** | 0.04 | 0.23 |
| ***trans*-Pt** | 0.18 | 2300 |
| ***cis*-Pd** | 0.08 | 3.6 |
| ***trans*-Pd** | 1.02 | 78000 |

[a]Upconversion quantum yield $\Phi_{UC}$. Excited with 635 ± 5 nm laser diode (central wavelength located at 639 nm, 55 mW). With the prompt fluorescence of methylene blue as the standard ($\Phi$ = 0.03 in methanol). *c*[sensitizers] = 3.0 $\mu$ M, *c*[rubrene] = 180 $\mu$M. In degassed toluene, 20 °C. [b]The overall upconversion capability $\eta = \varepsilon\Phi_{UC}$, $\varepsilon$ means the extinction coefficient at 639 nm in toluene.

Interestingly, if extinction coefficient was taken in account to evaluate the overall upconversion capability ($\eta$, $\eta = \varepsilon\cdot\Phi_{UC}$), proposed by Zhao and co-workers,[19] ***trans*-Pd** showed significantly larger $\eta$ value ($7.80 \times 10^4$ $M^{-1}cm^{-1}$) than the other 3 complexes (Table 2). More importantly, ***trans*-Pd** or **Pt *trans*** complex displays $\eta$ value $10^4$ times higher than the cis analogue. These results strongly suggested the importance of the orientation of $\beta$-oxazolone moieties on the triplet energy transfer process, as evidenced by the larger $\Phi_{UC}$s or $\eta$s in ***trans*-Pt/Pd** than *cis* analogues for the longer triplet lifetimes and Q-band absorptions.

## CONCLUSION

Taken together, we synthesized Pd and Pt complexes of *cis*- and *trans*-porphodilactones and investigated their photophysical properties related to the lowest triplet excited states. As expected, the gradually red-shifted absorption and NIR emission from metalloporphyrin, porpholactone, and *cis*/*trans*-porphodilactones were observed, indicating the number and orientation of $\beta$-oxazolone moieties influence their photophysical properties. ***cis*/*trans*-Pt/Pd** display remarkable Stokes shifts, which are comparable to tetrabenzoporphyrins and linearly $\pi$-expanded derivatives, demonstrating that $\beta$-lactonization efficiently lowers the lowest triplet states. The orientation of $\beta$-oxazolone moieties also affects the lowest triplet excited states of metalloporphyrinoids, which is evidenced by different C═O stretching vibration in excited states. Computational studies have been performed to provide insights into the electronic structures and spectroscopic properties of ***cis*/*trans*-Pt/Pd**, which offers a better understanding on the nature of the orientation of $\beta$-oxazolone moieties on the excited state energy. In addition, ***trans*-Pd/Pt** showed more efficient energy transfer to rubrene to generate delayed fluorescence than cis analogues in TTA reactions, suggesting the importance of subtle changes in porphyrin periphery on the photosensitizing ability. This work provides a benchmarked example of modulating NIR phosphorescence with the structural similarity, in contrast to the traditional "extended $\pi$-conjugation" strategies and would be important to design NIR porphyrinoids as optoelectronic materials, solar fuel, and photosensitizers.

## EXPERIMENTAL SECTION

Unless otherwise stated, all reactions were performed under an inert nitrogen atmosphere. UV−visible spectra were recorded on an Agilent 8453 UV−vis spectrometer equipped with an Agilent 89090A thermostat (±0.1 °C) at 25.0 °C. The emission spectra and lifetimes were recorded on an Edinburgh Analytical Instruments FLS920 lifetime and steady state spectrometer (450 W Xe lamp, PMT R928 and Hamamatsu R5509). Mass spectra were measured on a Bruker APEX IV FT-ICR Mass Spectrometer (ESI-MS). IR spectra were recorded on a Bruker Vector22 FT-IR spectrometer as KBr pellets. $^1$H NMR spectra were measured on a Bruker ARX400 (400 MHz) or AVANCE III (500 MHz) spectrophotometer; $^{19}$FNMR ($CF_3COOH$ as external standard) and $^{13}$C NMR spectra were recorded on a Bruker AVANCE III spectrophotometer (471 MHz for $^{19}$F, 126 MHz for $^{13}$C). For the optical measurements in liquid solution, spectroscopic-grade DCM, $CH_3CN$ and toluene were used as purchased from Alfa-Aesar.

**Synthesis of *trans* and *cis*-Pt.** *trans*- or *cis*-$H_2$ (80 mg, 0.079 mmol) and $Pt(acac)_2$ (155 mg, 5 equiv) were dissolved in 10 mL of PhCN and was refluxed for 48 h under $N_2$. The solvent was removed under reduced pressure. Then the mixture was dissolved in 5 mL of $CHCl_3/CH_3OH$ ($v/v$ = 1:1) mixing solvent, and excess $Zn(AcO)_2\cdot 2H_2O$ was added. The reaction mixture was refluxed for 3 h, and the remaining free base ligands were reacted. ***trans*-** and ***cis*-Pd** were obtained after silica column chromatography in the yield of 18 and 10%, respectively. ***trans*-Pt:** $^1$HNMR (400 MHz, $CDCl_3$) $\delta$ 8.67 (dd, $J$ = 17.2, 5.1 Hz, 4H); HRMS (ESI$^+$) $m/z$ [M + H]$^+$: calcd for $C_{42}H_5F_{20}N_4O_4Pt$ 1203.9639, found: 1203.9604. ***cis*-Pt:** $^1$H NMR (400 MHz, $CDCl_3$) $\delta$ 8.62 (s, 2H), 8.52 (s, 2H). HRMS (ESI$^+$) $m/z$ [M]$^+$: calcd for $C_{42}H_4F_{20}N_4O_4Pt$ 1202.9561, found: 1202.9560.

**Synthesis of *trans* and *cis*-Pd.** *trans*- or *cis*-$H_2$ (80 mg, 0.079 mmol) and $Pd(acac)_2$ (120 mg, 5 equiv) were dissolved in 10 mL of PhCN and was refluxed for 12 h under $N_2$. Then the solvent was


DOI: 10.1021/jacs.5b06332
J. Am. Chem. Soc. 2015, 137, 10745−10752

removed under reduced pressure. ***trans***- and ***cis***-**Pd** were obtained after silica column chromatography in the yield of 45 and 43%, respectively. ***trans***-**Pd**: $^1$H NMR (400 MHz, $CDCl_3$) $\delta$ 8.66 (s, 4H). HRMS ($ESI^+$) $m/z$ $[M]^+$: calcd for $C_{42}H_4F_{20}N_4O_4Pd$ 1113.8948, found: 1113.8927. ***cis***-**Pd**: $^1$H NMR (400 MHz, $CDCl_3$) $\delta$ 8.59 (s, 2H), 8.46 (s, 2H). HRMS ($ESI^+$) $m/z$ $[M]^+$: calcd for $C_{42}H_4F_{20}N_4O_4Pd$ 1113.8948, found: 1113.8948.

**Time-Resolved Infrared Spectroscopy.** The triplet excited state formation upon UV excitation was monitored by step-scan, time-resolved Fourier transform infrared (TR-FTIR) absorption spectroscopy.[20] The TR-FTIR instrument comprises a Nicolet Nexus 870 step-scan FTIR spectrometer, a Spectra Physics Lab170 Nd YAG laser, a pulse generator (Stanford Research DG535) to initiate the laser pulse and achieve synchronization of the laser with data collection, two digitizers (internal 100 kHz 16-bit digitizer and external 100 MHz 14-bit GAGE CS14100 digitizer) which offer fast time resolution and a wide dynamic range as needed, and a personal computer to control the whole experiment. The detector used in this work is the photovoltaic MCT (0.5 mm) equipped with a fast internal preamplifier (50 MHz).

There are two outputs from the detector: output DC, corresponding to the value of the static interferogram, and output AC, corresponding to the time-resolved change of the interferogram. The AC signal was then amplified by an external preamplifier (Stanford Research, SR560). The differential absorbance spectra is calculated based on equation:

$$\Delta A = A_{AC+DC} - A_{DC} = -\log_{10}(1 - \Delta I_{AC}/I_{DC})$$

where $I_{DC}$ and $\Delta I_{AC}$ are the single-beam intensity spectra corresponding to static (DC) and dynamic (AC) channels. $\Delta I_{AC}$ is calibrated before being used in the equation because different gain is applied to the AC channel.[20]

The third harmonic of Nd:YAG laser (355 nm) operating at 10 Hz repetition rate was used in the experiments. The laser excitation beam was directed through an iris aperture (3 mm in diameter) and then overlapped with the infrared beam in the sample cell within the sample compartment of the FTIR spectrometer. The laser beam energy after the aperture was 3 mJ per pulse. A Harrick flowing solution cell with 2 mm-thick $CaF_2$ windows (path-length: 500 $\mu$m) was used for the measurements. The closed flowing system is driven by a peristaltic pump (ColeParmer Masterflex) to refresh the sample before every laser pulse.

**Theoretical Calculations.** We carried out density functional theory calculations as implemented in the program package Gaussian 09[21] using the hybrid density functional theory, i.e., Becke's three-parameter nonlocal exchange functional with the nonlocal correlation functional of Lee, Yang, and Parr (B3LYP).[14] The cc-pvdz basis set was used for C, N, H, F, and O atoms, and the LANL2DZ[15] basis set was used for Pt and Pd atoms taking into account the relativistic effects implicitly. The geometries of the singlet and triplet Pt and Pd porphyrinoids were optimized, and the stationary points were identified as local minima using vibrational frequency calculations, which confirmed that all of the computed vibrational frequencies were real. The molecular orbitals and atomic polar tensors (APT) charges of Pt and Pd porphyrinoids in the singlet and triplet states were calculated at the same level. In general, DFT calculations with the B3LYP hybrid functional tend to overestimate the vibrational frequencies, so all calculated vibrational frequencies were scaled by a factor 0.9614, according to Koch and Holsthausen.[22]

**Upconversion Quantum Yields Measurement.** The upconversion quantum yields ($\Phi_{UC}$) of ***cis***-**Pt**, ***trans***-**Pt**, ***cis***-**Pd**, and ***trans***-**Pd** with rubrene were determined in degassed toluene with the prompt fluorescence of the methylene blue ($\Phi_f$ = 0.03 in methanol) as standard and calculated with the following equation:[17a]

$$\Phi_{UC} = 2\Phi\mathrm{std}\left(\frac{A_{std}}{A_{unk}}\right)\left(\frac{I_{unk}}{I_{std}}\right)\left(\frac{\eta_{unk}}{\eta_{std}}\right)^2$$

where $\Phi_{UC}$, $A_{unk}$, and $I_{unk}$ represents the quantum yield, absorbance, and integrated photoluminescence intensity; $\eta_{unk}$ represents the refractive indices of the solvent used for the samples; and symbols with "std" stand for the corresponding parameter for the standard.

## ■ ASSOCIATED CONTENT

### Supporting Information

These materials are available free of charge via the Internet at The Supporting Information is available free of charge on the ACS Publications website at DOI: 10.1021/jacs.5b06332.

Transient absorption spectra; cyclic voltammetry data; Stern−Volmer analysis; and $^1$H NMR, $^{13}$C NMR, $^{19}$F NMR, IR and ESI-MS spectra (PDF)

Photophysical data of metalloporphyrins (CIF)

Photophysical data of porpholactones (CIF)

## ■ AUTHOR INFORMATION


### Corresponding Authors

*E-mail: hongmei@iccas.ac.cn.

*E-mail: zhangjunlong@pku.edu.cn.


### Notes

The authors declare no competing financial interest.

## ■ ACKNOWLEDGMENTS

Support from National Key Basic Research Support Foundation of China (NKBRSFC) (2010CB912302, 2015CB856300), NSFC (Grant Nos. 20971007, 21271013, and 21321001 to J.L.Z. and Grant Nos. 21333012 and 21425313 to H.S.), and CAS project XDB12020200 is gratefully acknowledged.

## ■ REFERENCES


(1) (a) *Handbook of Porphyrin Science*; Kadish, K. M., Smith, K. M., Guilard, R., Eds.; World Scientific Publishing: Singapore, 2010. (b) Ethirajan, M.; Chen, Y. H.; Joshi, P.; Pandey, R. K. *Chem. Soc. Rev.* **2011**, *40*, 340. (c) Tanaka, T.; Osuka, A. *Chem. Soc. Rev.* **2015**, *44*, 943. (d) Bottari, G.; de la Torre, G.; Torres, T. *Acc. Chem. Res.* **2015**, *48*, 900.

(2) (a) Jasat, A.; Dolphin, D. *Chem. Rev.* **1997**, *97*, 2267. (b) Sessler, J. L.; Seidel, D. *Angew. Chem., Int. Ed.* **2003**, *42*, 5134. (c) Toganoh, M.; Furuta, H. *Chem. Commun.* **2012**, *48*, 937. (d) Roznyatovskiy, V. V.; Lee, C.-H.; Sessler, J. L. *Chem. Soc. Rev.* **2013**, *42*, 1921. (e) Mori, H.; Tanaka, T.; Osuka, A. *J. Mater. Chem. C* **2013**, *1*, 2500. (f) Carvalho, C. M. B.; Brocksom, T. J.; de Oliveira, K. T. *Chem. Soc. Rev.* **2013**, *42*, 3302.

(3) (a) Kobayashi, N.; Konami, H. *J. Porphyrins Phthalocyanines* **2001**, *05*, 233. (b) Nguyen, K. A.; Pachter, R. *J. Chem. Phys.* **2001**, *114*, 10757. (c) Rogers, J. E.; Nguyen, K. A.; Hufnagle, D. C.; McLean, D. G.; Su, W. J.; Gossett, K. M.; Burke, A. R.; Vinogradov, S. A.; Pachter, R.; Fleitz, P. A. *J. Phys. Chem. A* **2003**, *107*, 11331. (d) Mack, J.; Asano, Y.; Kobayashi, N.; Stillman, M. J. *J. Am. Chem. Soc.* **2005**, *127*, 17697. (e) Yamada, H.; Kuzuhara, D.; Takahashi, T.; Shimizu, Y.; Uota, K.; Okujima, T.; Uno, H.; Ono, N. *Org. Lett.* **2008**, *10*, 2947. (f) Graham, K. R.; Yang, Y.; Sommer, J. R.; Shelton, A. H.; Schanze, K. S.; Xue, J.; Reynolds, J. R. *Chem. Mater.* **2011**, *23*, 5305.

(4) (a) *Advances in Photosynthesis and Respiration*; Grimm, B., Porra, R., Rüdiger, W., Scheer, H., Eds.; Springer: Dordrecht, 2006; Vol. 25: Chlorophyllsand Bacteriochlorophylls. (b) Chen, M.; Schliep, M.; Willows, R. D.; Cai, Z.-L.; Neilan, B. A.; Scheer, H. *Science* **2010**, *329*, 1318. (c) Chen, M. *Annu. Rev. Biochem.* **2014**, *83*, 317. (d) Li, Y.; Chen, M. *Funct. Plant Biol.* **2015**, *42*, 493.

(5) (a) Kee, H. L.; Kirmaier, C.; Tang, Q.; Diers, J. R.; Muthiah, C.; Taniguchi, M.; Laha, J. K.; Ptaszek, M.; Lindsey, J. S.; Bocian, D. F.; Holten, D. *Photochem. Photobiol.* **2007**, *83*, 1110. (b) Kee, H. L.; Kirmaier, C.; Tang, G.; Diers, J. R.; Muthiah, C.; Taniguchi, M.; Laha, J. K.; Ptaszek, M.; Lindsey, J. S.; Bocian, D. F.; Holten, D. *Photochem. Photobiol.* **2007**, *83*, 1125. (c) Springer, J. W.; Faries, K. M.; Diers, J. R.; Muthiah, C.; Mass, O.; Kee, H. L.; Kirmaier, C.; Lindsey, J. S.;




DOI: 10.1021/jacs.5b06332
J. Am. Chem. Soc. 2015, 137, 10745−10752

Bocian, D. F.; Holten, D. *Photochem. Photobiol.* **2012**, *88*, 651. (d) Yuen, J. M.; Harris, M. A.; Liu, M.; Diers, J. R.; Kirmaier, C.; Bocian, D. F.; Lindsey, J. S.; Holten, D. *Photochem. Photobiol.* **2015**, *91*, 331.
(6) (a) Telfer, A. *Plant Cell Physiol.* **2014**, *55*, 1216. (b) Erickson, E.; Wakao, S.; Niyogi, K. K. *Plant J.* **2015**, *82*, 449.
(7) Ke, X. S.; Chang, Y.; Chen, J. Z.; Tian, J. W.; Mack, J.; Cheng, X.; Shen, Z.; Zhang, J. L. *J. Am. Chem. Soc.* **2014**, *136*, 9598.
(8) Che, C.-M.; Hou, Y.-J.; Chan, M. C. W.; Guo, J.; Liu, Y.; Wang, Y. *J. Mater. Chem.* **2003**, *13*, 1362.
(9) (a) Khalil, G.; Gouterman, M.; Ching, S.; Costin, C.; Coyle, L.; Gouin, S.; Green, E.; Sadilek, M.; Wan, R.; Yearyean, J.; Zelelow, B. *J. Porphyrins Phthalocyanines* **2002**, *06*, 135. (b) McCarthy, J. R.; Jenkins, H. A.; Brückner, C. *Org. Lett.* **2003**, *5*, 19. (c) Akhigbe, J.; Ryppa, C.; Zeller, M.; Brückner, C. *J. Org. Chem.* **2009**, *74*, 4927. (d) Khalil, G. E.; Daddario, P.; Lau, K. S. F.; Imtiaz, S.; King, M.; Gouterman, M.; Sidelev, A.; Puran, N.; Ghandehari, M.; Brückner, C. *Analyst* **2010**, *135*, 2125. (e) Brückner, C.; Ogikubo, J.; McCarthy, J. R.; Akhigbe, J.; Hyland, M. A.; Daddario, P.; Worlinsky, J. L.; Zeller, M.; Engle, J. T.; Ziegler, C. J.; Ranaghan, M. J.; Sandberg, M. N.; Birge, R. R. *J. Org. Chem.* **2012**, *77*, 6480. (f) Ogikubo, J.; Meehan, E.; Engle, J. T.; Ziegler, C. J.; Brückner, C. *J. Org. Chem.* **2012**, *77*, 6199. (g) Ogikubo, J.; Meehan, E.; Engle, J. T.; Ziegler, C. J.; Brückner, C. *J. Org. Chem.* **2013**, *78*, 2840.
(10) Pineiro, M.; Carvalho, A. L.; Pereira, M. M.; Gonsalves, A.; Arnaut, L. G.; Formosinho, S. J. *Chem. - Eur. J.* **1998**, *4*, 2299.
(11) Sommer, J. R.; Shelton, A. H.; Parthasarathy, A.; Ghiviriga, I.; Reynolds, J. R.; Schanze, K. S. *Chem. Mater.* **2011**, *23*, 5296.
(12) (a) Alexandre, M. T. A.; Lührs, D. C.; van Stokkum, I. H. M.; Hiller, R.; Groot, M.-L.; Kennis, J. T. M.; van Grondelle, R. *Biophys. J.* **2007**, *93*, 2118. (b) Di Donato, M.; Groot, M. L. *Biochim. Biophys. Acta, Bioenerg.* **2015**, *1847*, 2.
(13) Silverstein, R. M.; Webster, F. X.; Kiemle, D. J. *Spectrometric Identification of Organic Compounds*, 7th ed.; John Wiley and Sons: New York, 2005.
(14) (a) Gonzalez, C.; Schlegel, H. B. *J. Phys. Chem.* **1990**, *94*, 5523. (b) Becke, A. D. *J. Chem. Phys.* **1993**, *98*, 5648.
(15) Hay, P. J.; Wadt, W. R. *J. Chem. Phys.* **1985**, *82*, 299.
(16) Cioslowski, J. *J. Am. Chem. Soc.* **1989**, *111*, 8333.
(17) (a) Singh-Rachford, T. N.; Castellano, F. N. *Coord. Chem. Rev.* **2010**, *254*, 2560. (b) Deng, F.; Sommer, J. R.; Myahkostupov, M.; Schanze, K. S.; Castellano, F. N. *Chem. Commun.* **2013**, *49*, 7406.
(18) (a) Olmsted, J. *J. Phys. Chem.* **1979**, *83*, 2581. (b) Singh-Rachford, T. N.; Haefele, A.; Ziessel, R.; Castellano, F. N. *J. Am. Chem. Soc.* **2008**, *130*, 16164.
(19) Zhao, J.; Ji, S.; Guo, H. *RSC Adv.* **2011**, *1*, 937.
(20) (a) Uhmann, W.; Becker, A.; Taran, C.; Siebert, F. *Appl. Spectrosc.* **1991**, *45*, 390. (b) Drapcho, D. L.; Curbelo, R.; Jiang, E. Y.; Crocombe, R. A.; McCarthy, W. J. *Appl. Spectrosc.* **1997**, *51*, 453. (c) Zou, X.; Dai, X.; Liu, K.; Zhao, H.; Song, D.; Su, H. *J. Phys. Chem. B* **2014**, *118*, 5864.
(21) Frisch, M. J. et al. *Gaussian 09*, revision B.01; Gaussian, Inc.:Wallingford, CT, 2009. The complete reference is shown in the Supporting Information.
(22) Koch, W.; Holthausen, M. C. *A Chemist's Guide to Density Functional Theory*; 2nd ed.; Wiley-VCH Verlag GmbH: Berlin, 2001; p 134.


DOI: 10.1021/jacs.5b06332
*J. Am. Chem. Soc.* 2015, 137, 10745−10752